C h a p t e r 5

5 APPLICATION TO FIELD DATA

"The bitterness of low quality remains long after the sweetness of low price is long forgotten."

(Benjamin Franklin, 1706-1790)

5.1 Introduction

This chapter contains results of S-layer differential transform applied to two data sets, one from a ground survey and one from an airborne survey. The ground survey covers an area of roughly 2km by 6km at low resolution (50m or 100m station spacing) with the intent to identify locations of conductors for follow-up work. The airborne data consists of a very high resolution (3m station spacing on average) line over an easily recognizable conductor and the purpose is to determine the depth and orientation of this body. Both survey geometries conformed to the central loop sounding configuration.

5.2 Ground survey

5.2.1 Data acquisition and system parameters

The data used were acquired in a sedimentary environment which has undergone various metamorphic events resulting in complex structural features. A TDEM in-loop survey was done across a mountain (Figure 5-1). The data acquisition was done under extreme field conditions. The station- and line-spacing varied across the survey area (mostly 100m line- and 50m station spacing). The grid that was surveyed is given in Figure 5-2. A total of 1543 stations were surveyed. At each station both the high and medium frequencies were utilized on the transmitter. The survey was done using a GEONICS EM57 transmitter and PROTEM receiver with a single component receiver coil. Parameters used for the survey are:

Frequency*:* 25 and 6.25Hz

Transmitter Loop Area: Single Turn 100x100m

Transmitter current: 14.5 A

Component: Vertical (z)

Synchronization: Reference cable.

Power Supply: 1,000W 110/220V, 50/60 (Hz single-phase motor-generator)

Current Waveform: Bipolar rectangular current with 50% duty cycle

Effective surface area of receiver coil: $100m^2$

Receiver Size: 34 x 38 x 27 cm

Figure 5-1: Mountain with TDEM survey team.

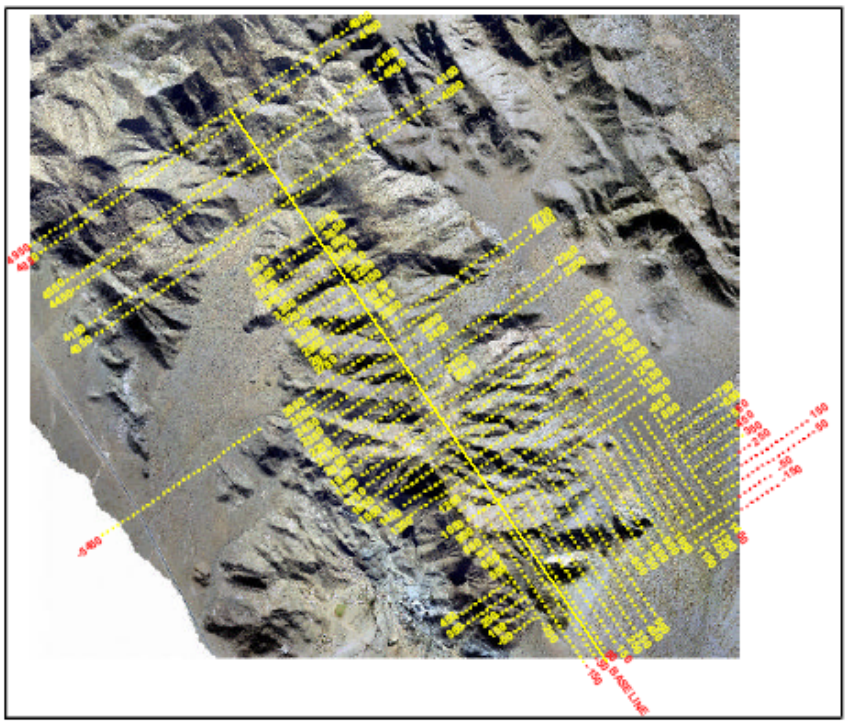

Figure 5-2: Grid locality and layout.

5.2.2 Objective

Based on the TDEM and other investigations (including geochemical and structural geological interpretations) some exploration boreholes were drilled and follow-up borehole TDEM surveys were done. This chapter is not intended to be a discussion of the exploration program or to propose a geological model for the area. The TDEM data acquired during this project are used to illustrate the performance of the S-layer differential transform under extremely challenging geological and topographical conditions.

5.2.3 Application of S-layer differential transform

The main challenge of applying an automated processing sequence to field data is noise. Even though system parameters can be chosen (McNeill, 1995) to optimise the signal to noise ratio, there will always be some stations in a large data set not conforming to the ideal TDEM decay behaviour. This can be due to random atmospheric noise, cultural

noise or geological noise. Whatever the cause, noise in data will produce noise in the processed product and in extreme cases may even cause a technique to fail. The S-layer differential transform is especially sensitive to noise because of the numerical differentiations performed. In addition to the optimal smoothing of data (chapter 4) a filter is also applied to *remove* noisy data points from each sounding before the transform is applied. Noise in a sounding curve is easily recognised through visual inspection of data, especially if presented in the logarithmic domain, by the sometimes random decay behaviour of the later time channels. A filter mimicking this visual inspection is achieved by computing the straight line regression coefficients for trios of data points starting from the last three channels and working back to the front. When the regression coefficient is larger than a specified value (0.997 default) it means that data conform to late time decay behaviour. (This test is performed in both the logarithmic and semi-logarithmic domains.) All data points after this channel are discarded as noise. Supplementary to that, the first appropriate positive data value is chosen as the first point for each sounding. This is done to negate the effect of sign changes sometimes manifesting in the early channels. Examples of the application of this filter as well as the "S-layer differential transform compatibility" (SDTC) filter (section 4.4.4) are shown in Figures 5-3 to 5-7.

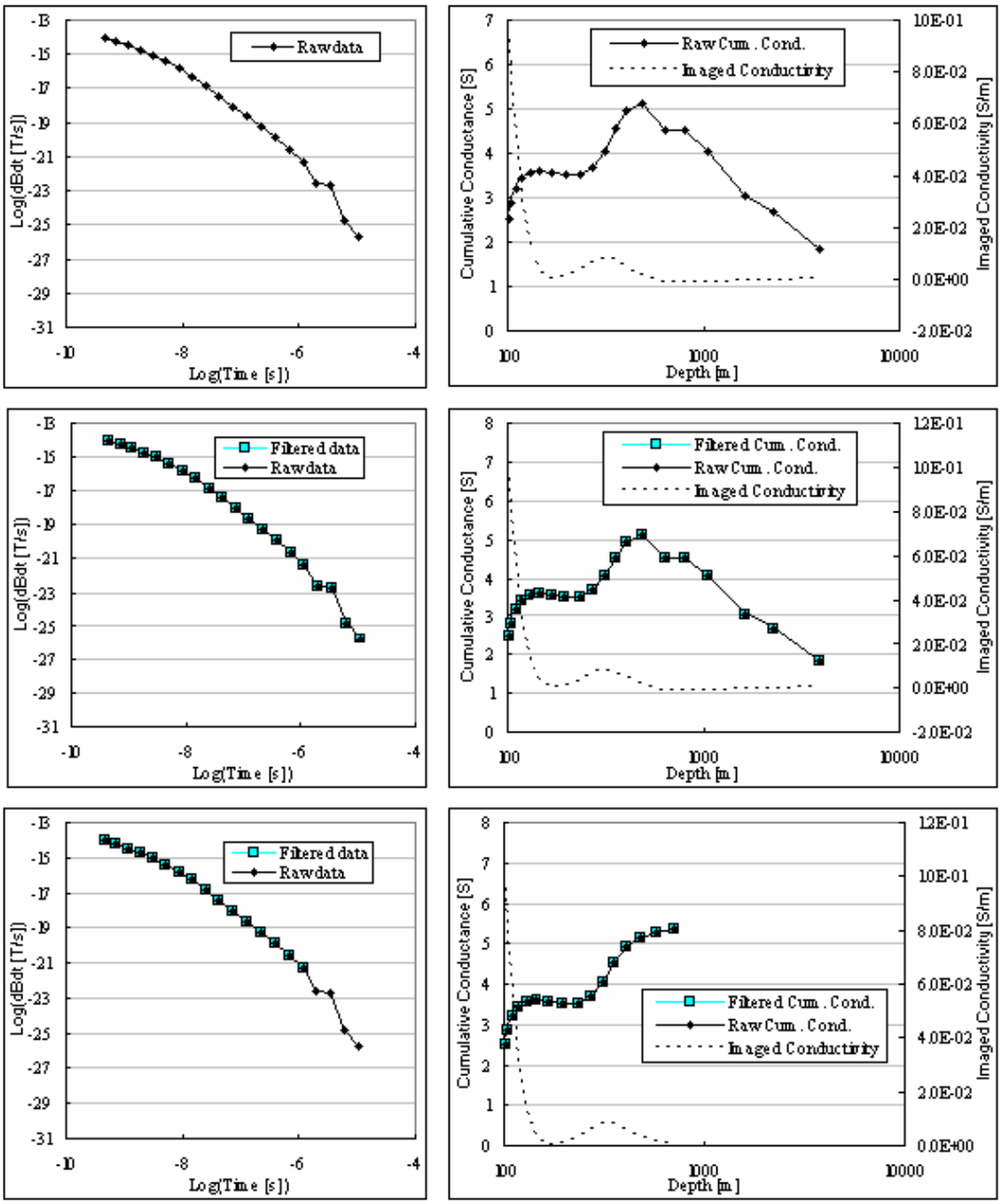

Figure 5-3: Line 4950, Station 100. ***Top:*** **Raw data with calculated cumulative conductance and imaged conductivity.** ***Middle:*** **No filter effect on input data values, only on cumulative conductance curve with imaged conductivity of filtered conductance values.** ***Bottom:*** **Input data filtered for late channel erratic behaviour and filtered cumulative conductance values.**

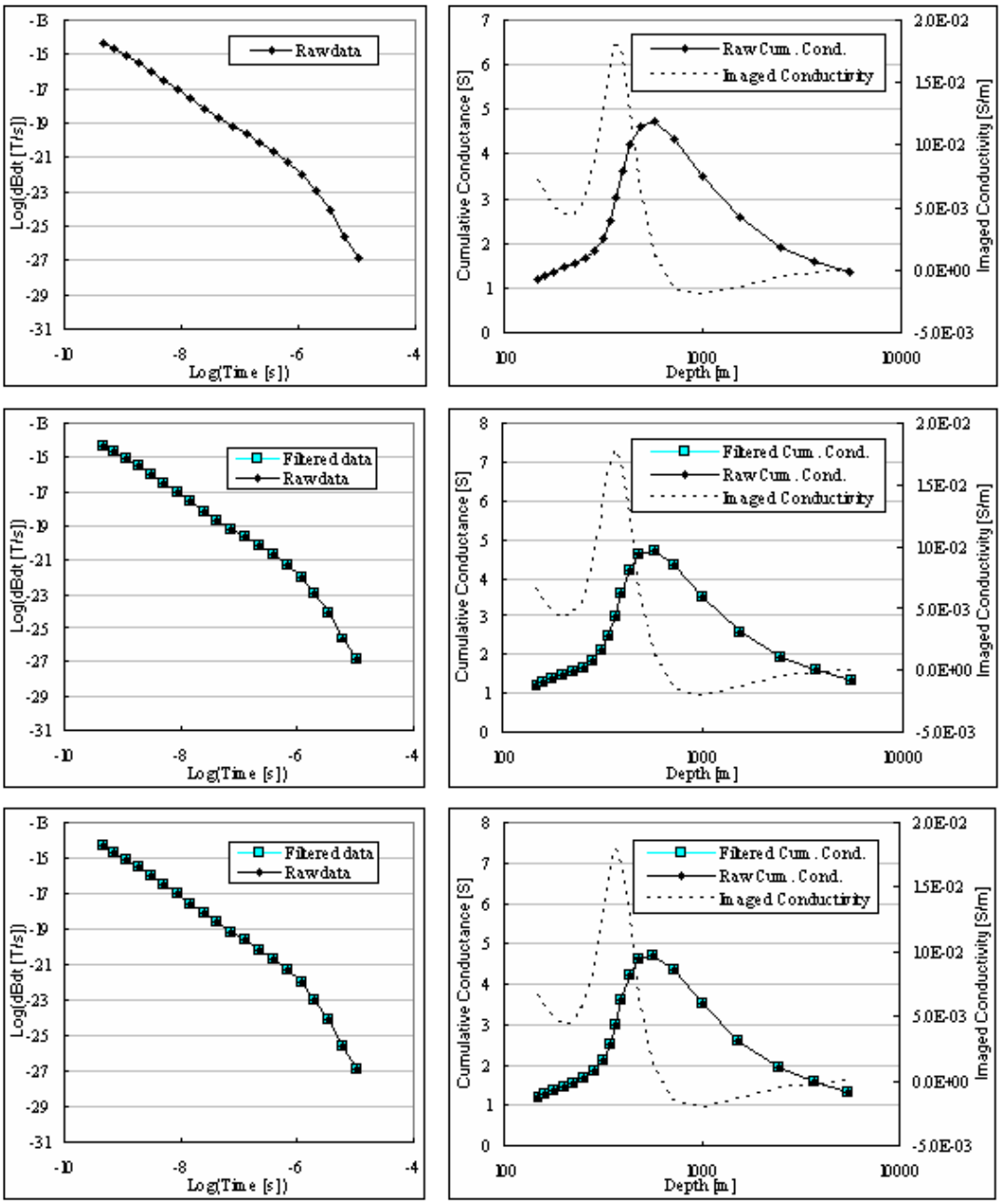

Figure 5-4: Line 4950, Station 300. ***Top:*** **Raw data with calculated cumulative conductance and imaged conductivity.** ***Middle:*** **No filter effect on input data values, only on cumulative conductance curve with imaged conductivity of filtered conductance values.** ***Bottom:*** **Input data filtered for late channel erratic behaviour and filtered cumulative conductance values.**

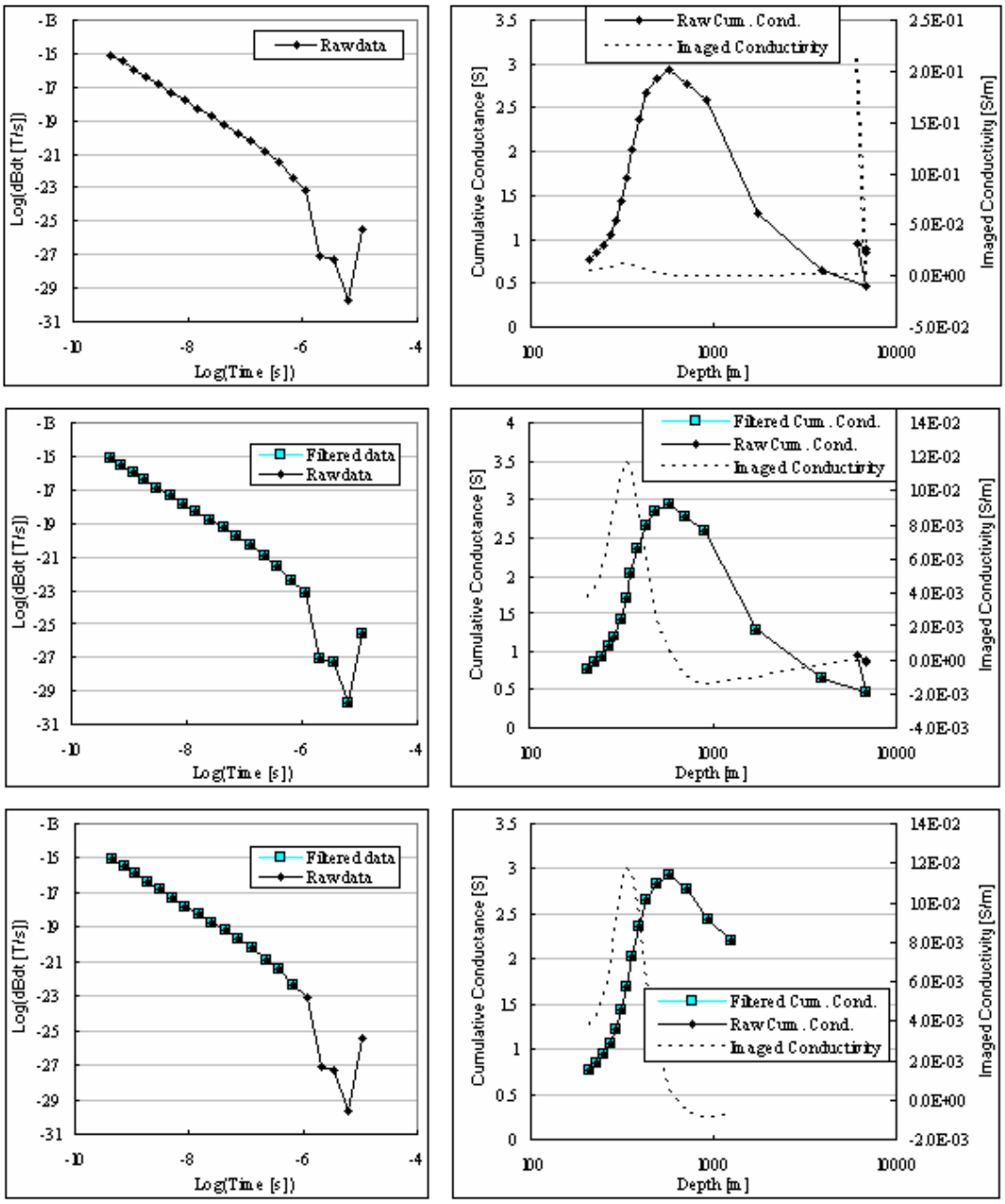

Figure 5-5: Line 4950, Station 400. ***Top:*** **Raw data with calculated cumulative conductance and imaged conductivity.** ***Middle:*** **No filter effect on input data values, only on cumulative conductance curve with imaged conductivity of filtered conductance values.** ***Bottom:*** **Input data filtered for late channel erratic behaviour and filtered cumulative conductance values.**

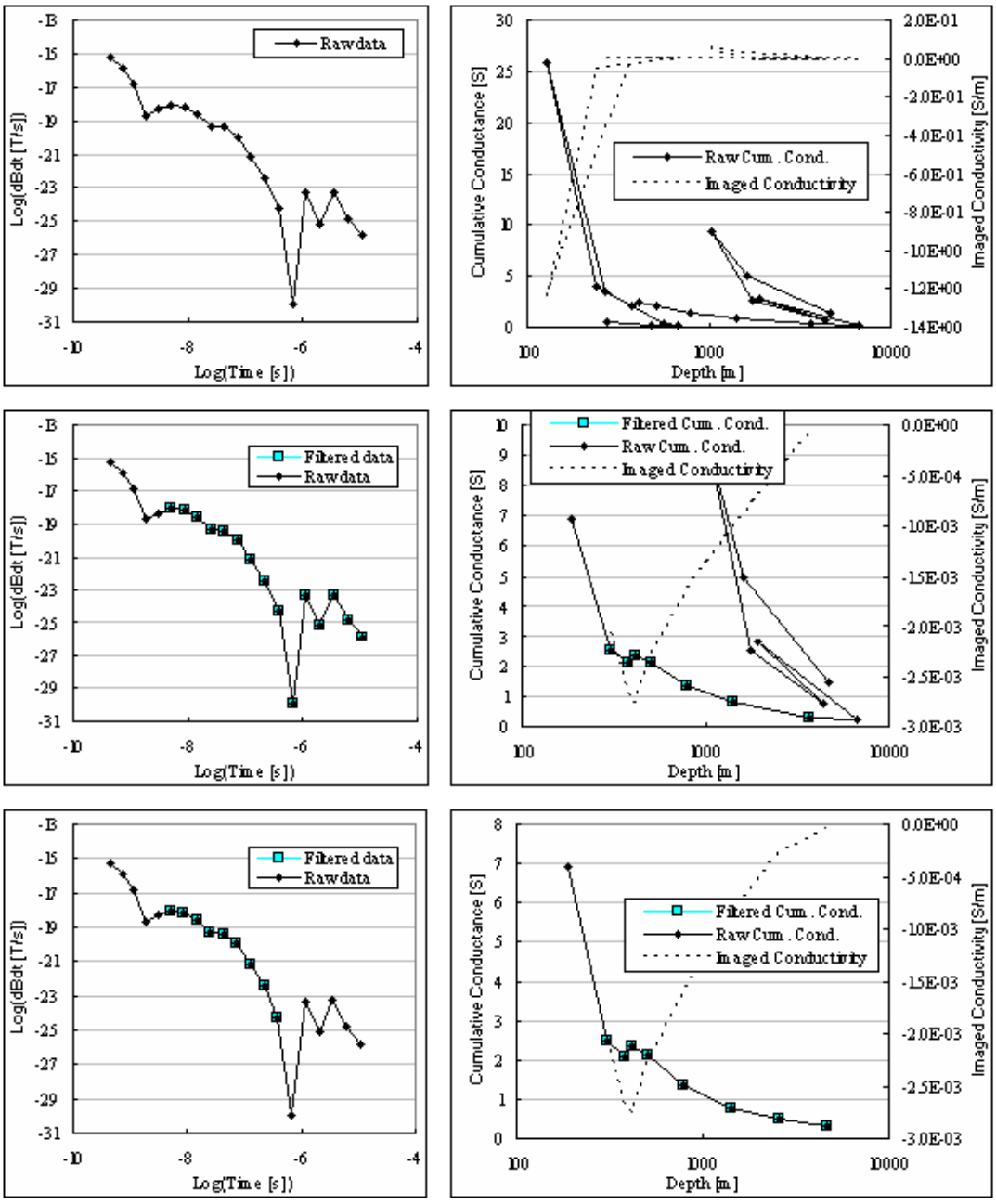

Figure 5-6: Line 4950, Station 450. ***Top:*** **Raw data with calculated cumulative conductance and imaged conductivity.** ***Middle:*** **No filter effect on input data values, only on cumulative conductance curve with imaged conductivity of filtered conductance values.** ***Bottom:*** **Input data filtered for late channel erratic behaviour and filtered cumulative conductance values.**

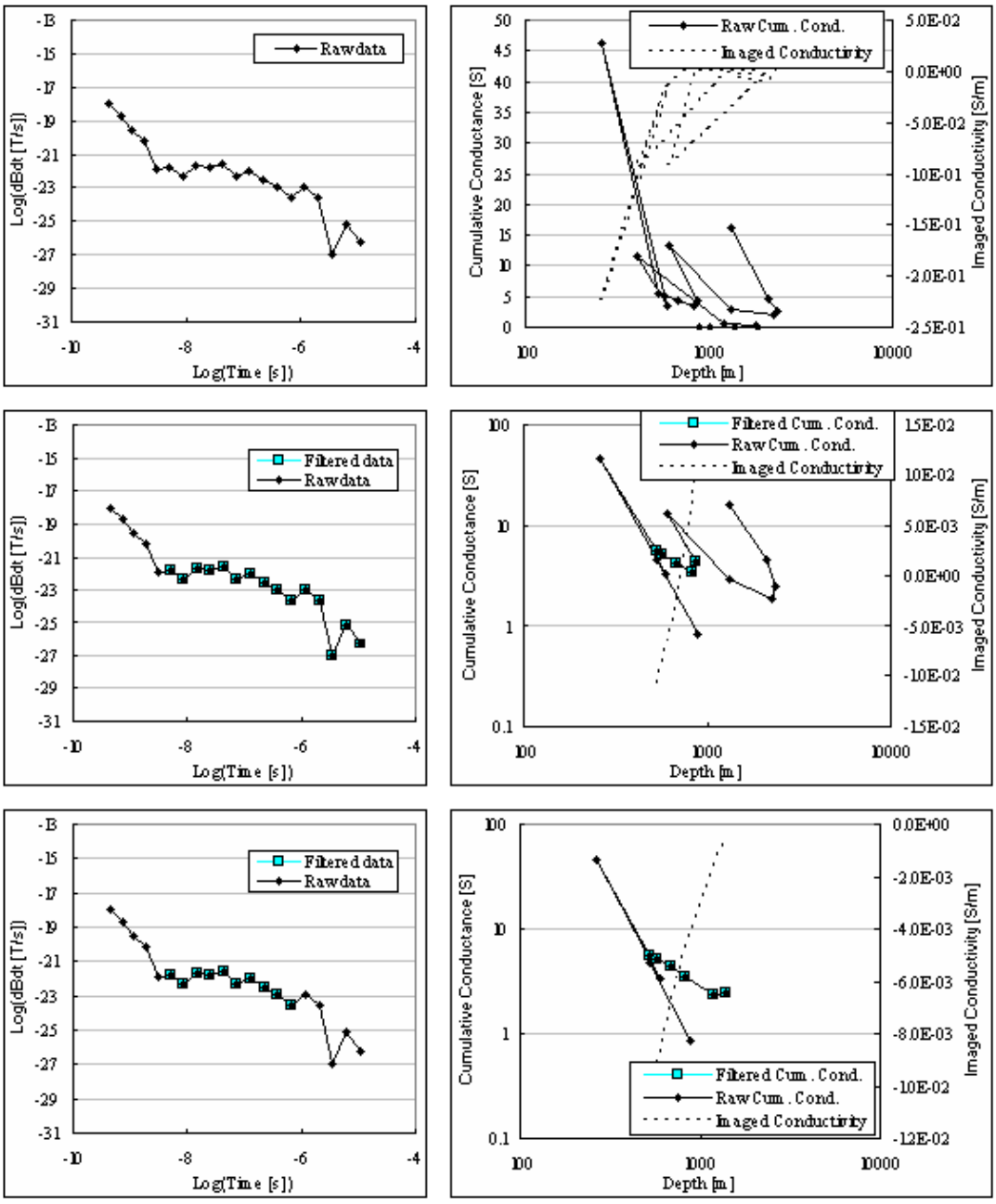

Figure 5-7: Line 4950, Station -1550. ***Top:*** **Raw data with calculated cumulative conductance and imaged conductivity.** ***Middle:*** **No filter effect on input data values, only on cumulative conductance curve with imaged conductivity of filtered conductance values.** ***Bottom:*** **Input data filtered for late channel erratic behaviour and filtered cumulative conductance values.**

Station 300 (Figure 5-4) has the smoothest input data, no data are filtered out and the final result (imaged conductivity) of the three processing options are identical. Station

100 (Figure 5-3) contains four data points at the end that are filtered out. No data are discarded by the SDTC filter and therefore the first two options yield identical results. The advantages of filtering out the last four points (17-20) are:

a more realistic maximum depth of investigation (706 m instead of 3943 m)

data points 15 and 16 still indicate high conductance values in the third case while in the first two cases they have been "contaminated" during smoothing by the consecutive noisy points to give lower than expected conductance values.

Similar results are observed for stations 400, 450 and -1550.

From these examples it is seen that the SDTC filter on its own also serves to discard some of the last erratic data points although it was not originally designed with this in mind. However, it is not as effective as removing the noisy points from the raw input data.

A final comparison of the second and third filter options are done by means of contoured imaged conductivity sections of line 4950. *(Note: This line has been chosen specifically because it contains stations with clean as well as noisy data.)* These sections are shown in Figure 5-8. Only imaged conductivities at depths of less than 800 m below the surface were contoured; deeper than that the data plot as individual, incoherent points and is not suitable for contouring. There is not much to choose between the two approaches when presented in this way. The only significant difference occurs between stations 400 to 600. Here the application of only the SDTC filter results in fairly high negative values (dark blue). The same feature is visible on the bottom section (SDTC plus noise filter) but it is less pronounced. Taking into account the fact that there are only three points on station 500, it is probably due to noisy data (see station 450, Figure 5-6) and the smoother, double filtered bottom section is preferable to the top one.

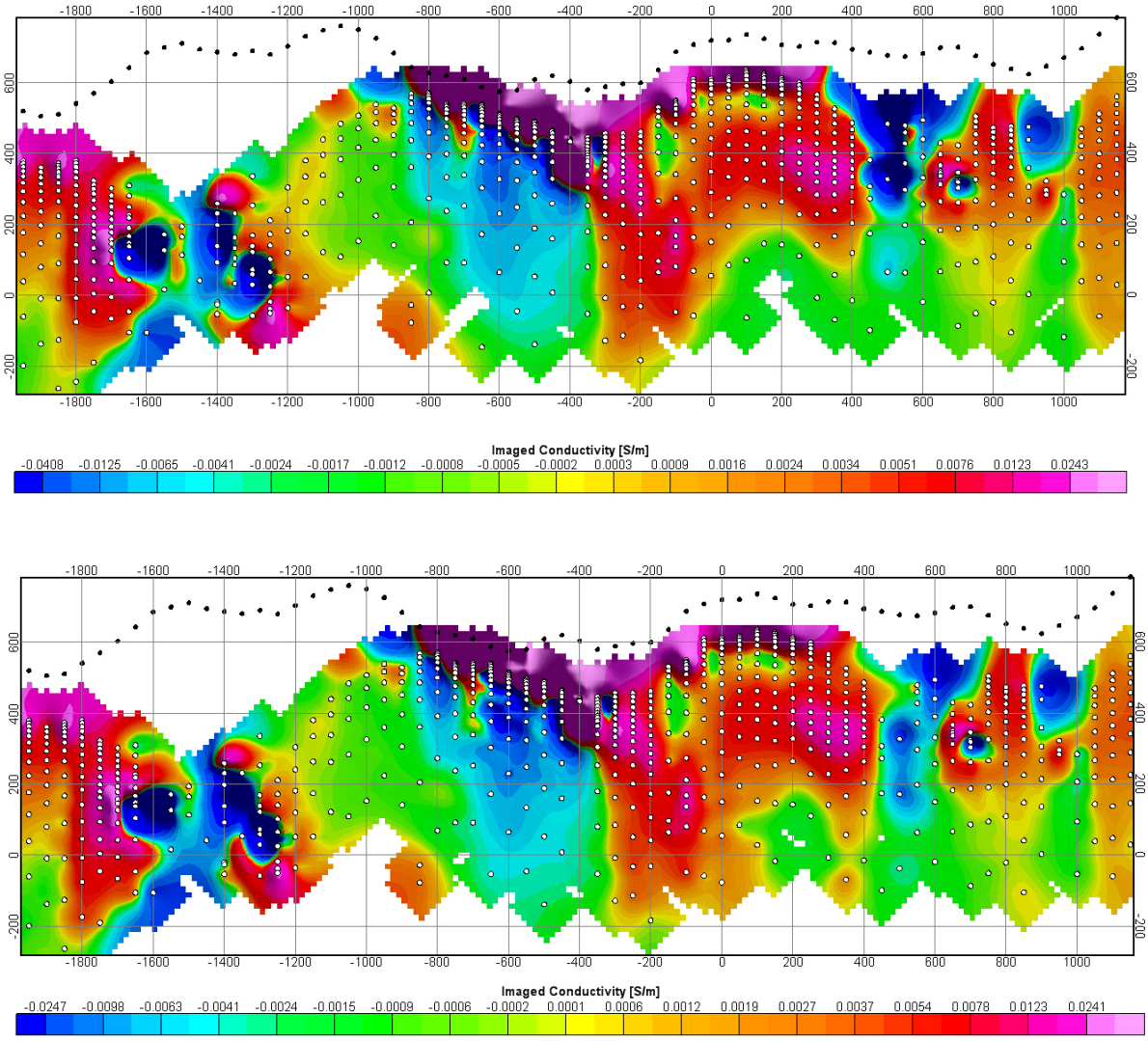

Figure 5-8: Comparison of SDTC filter only (top) and SDTC with additional noise filter (bottom). Black dots are station elevations (DTM) and white dots represent depths at which conductivities are calculated.

5.2.4 Comparison of 25Hz (high, H) and 6.25Hz (medium, M) base frequency data

The high frequency time channels range from 0.088ms to 6.978ms and the medium frequency channels from 0.35ms to 27.92ms. The first 14 channels of the medium frequency overlap with the last 13 of the high frequency. Measuring at these two frequencies therefore increases the coverage of the decay curve in terms of time, but also provides a check on the quality of data in the overlapping region. Often one frequency

will be noisier than the other in the overlapping range. If data quality is good for both frequencies, the conductivity depth sections obtained from the different frequencies should also overlap for intermediate depths with the high frequencies adding shallower data and the medium frequencies contributing to the deeper parts of the sections. Two lines are used to illustrate examples of poor and good correlations between these frequencies and to determine the reasons for discrepancies. Figure 5-9 is an example of good correlation between the sections obtained from the two frequencies. Three areas of interest are indicated by blocks A, B and C. In block A, a conductor is seen on both the high and medium frequencies.

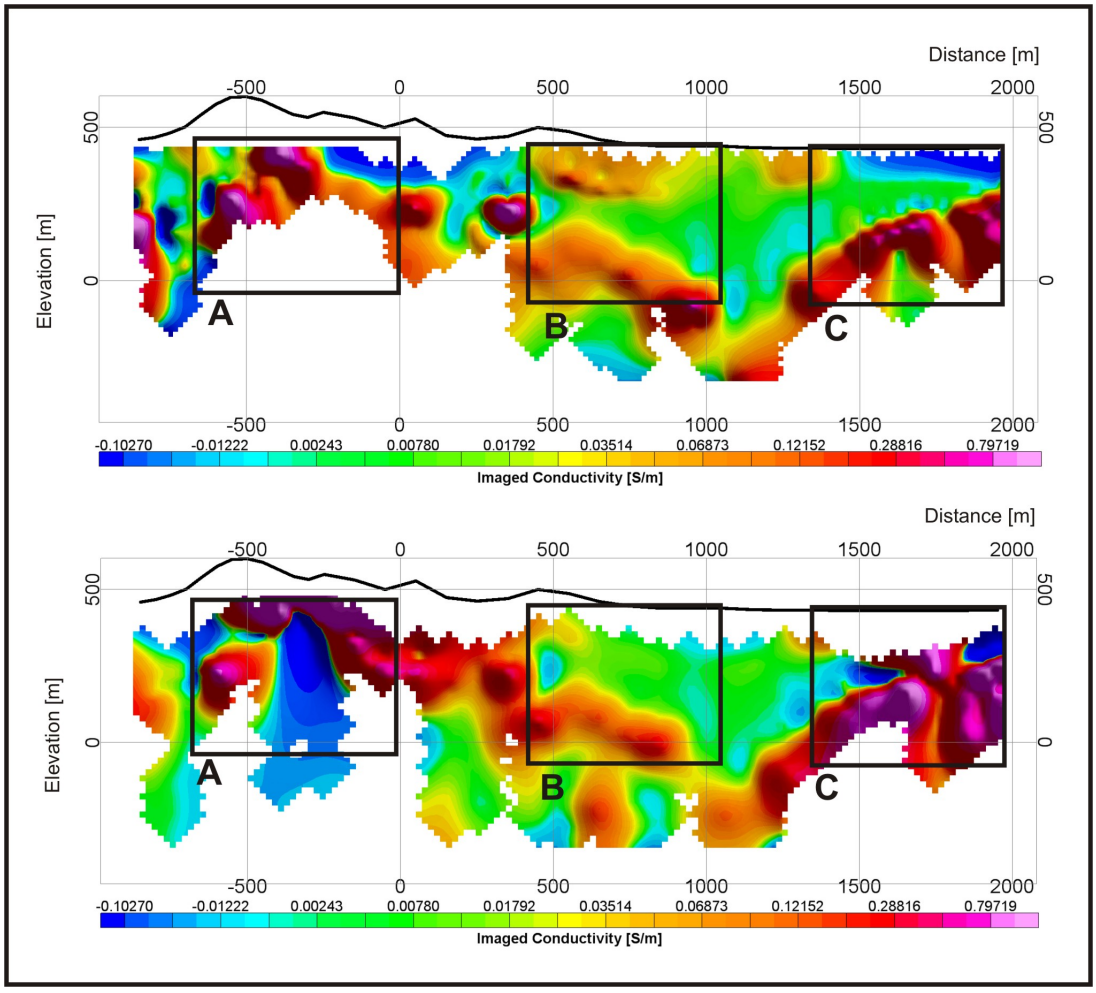

Figure 5-9: Line 450N showing good correlation between conductivity depth sections obtained from the high (top) and medium frequencies (bottom).

The top of the conductor is defined better by the high frequency. The medium frequency shows behaviour as in Figure 4-44 where it was found that when a conductor is shallower than the depth to where the 1st channel would plot in the surrounding half space (compare the depths of the first channel plots on the rest of the line), the cumulative conductance and conductivity curves are distorted. Block B indicates the capability of the method and the algorithm to map a deep conductor below a shallower one provided the right time channels are measured (two conductors on high frequency, only one visible on medium frequency). Block C indicates a good match between the frequencies with the medium frequency data containing some noise.

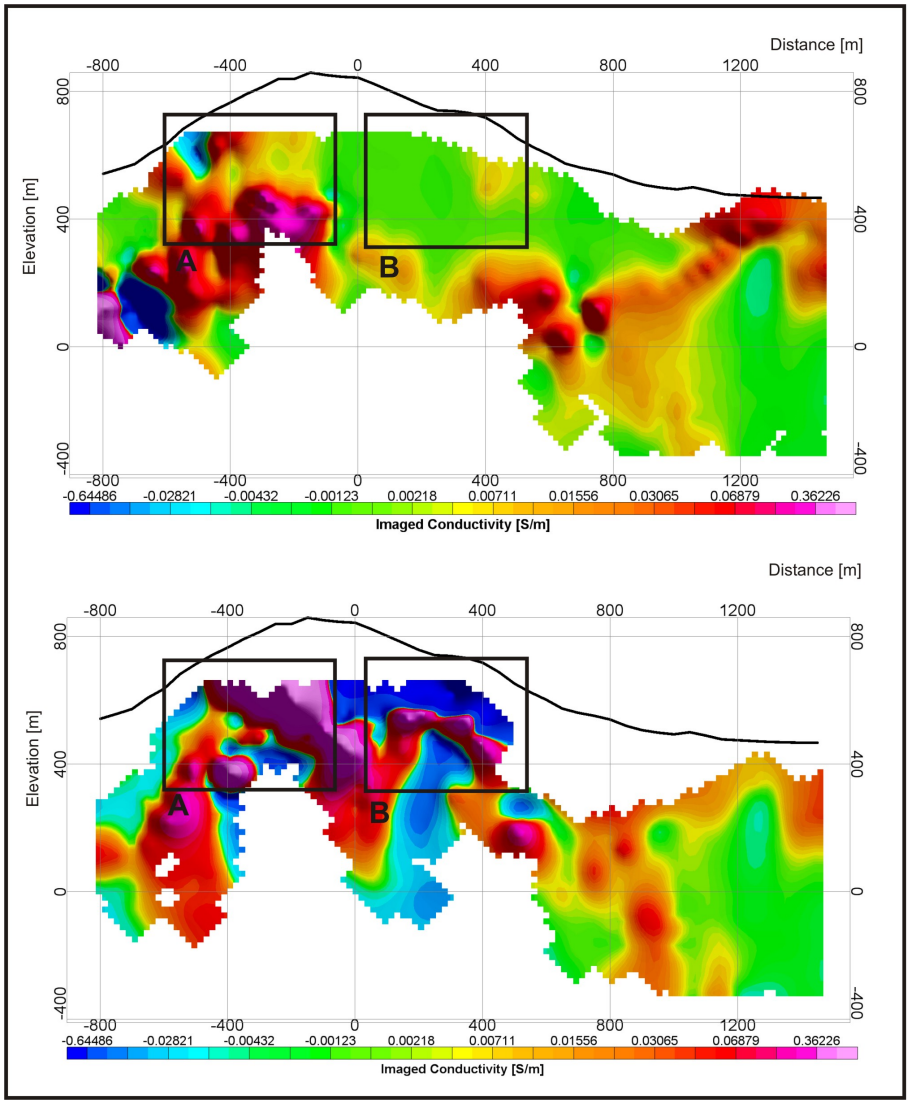

Figure 5-10: Line 1650N showing poor correlation between the high (top) and medium frequencies (bottom).

Figure 5-10 shows an example of poor correlation between conductivity depth sections for the two frequencies. In block A conductors are mapped on both frequencies but with more than 100m discrepancy in depth. In block B a conductor is mapped consistently over at least 4 stations on the medium frequency, but nothing is seen on the high frequency although this depth range is well covered. The question is where exactly these discrepancies originate. Figure 5-11 shows graphs of the measured data on line 450N for both frequencies and Figure 5-12 shows the same for line 1650N. It is clear that when the measured data correspond well (line 450N) the conductivity depth sections match. The reason for the discrepancies between dB/dt values for the medium and high frequencies of line 1650N is not known, but the behaviour of both frequencies is consistent over four adjacent stations (200m) implying a geological cause and not acquisition or processing error.

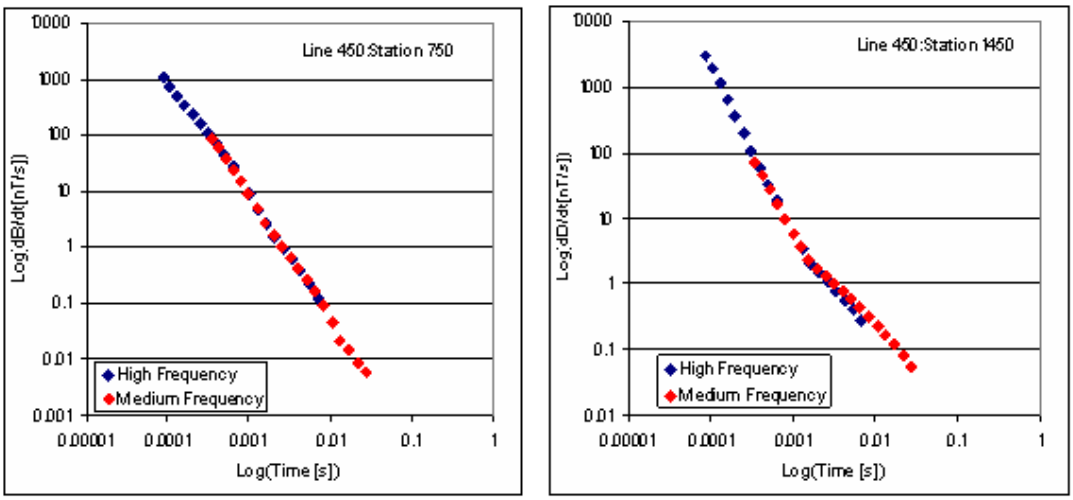

Figure 5-11: Line 450; Stations750 and 1450; medium and high frequency measured data.

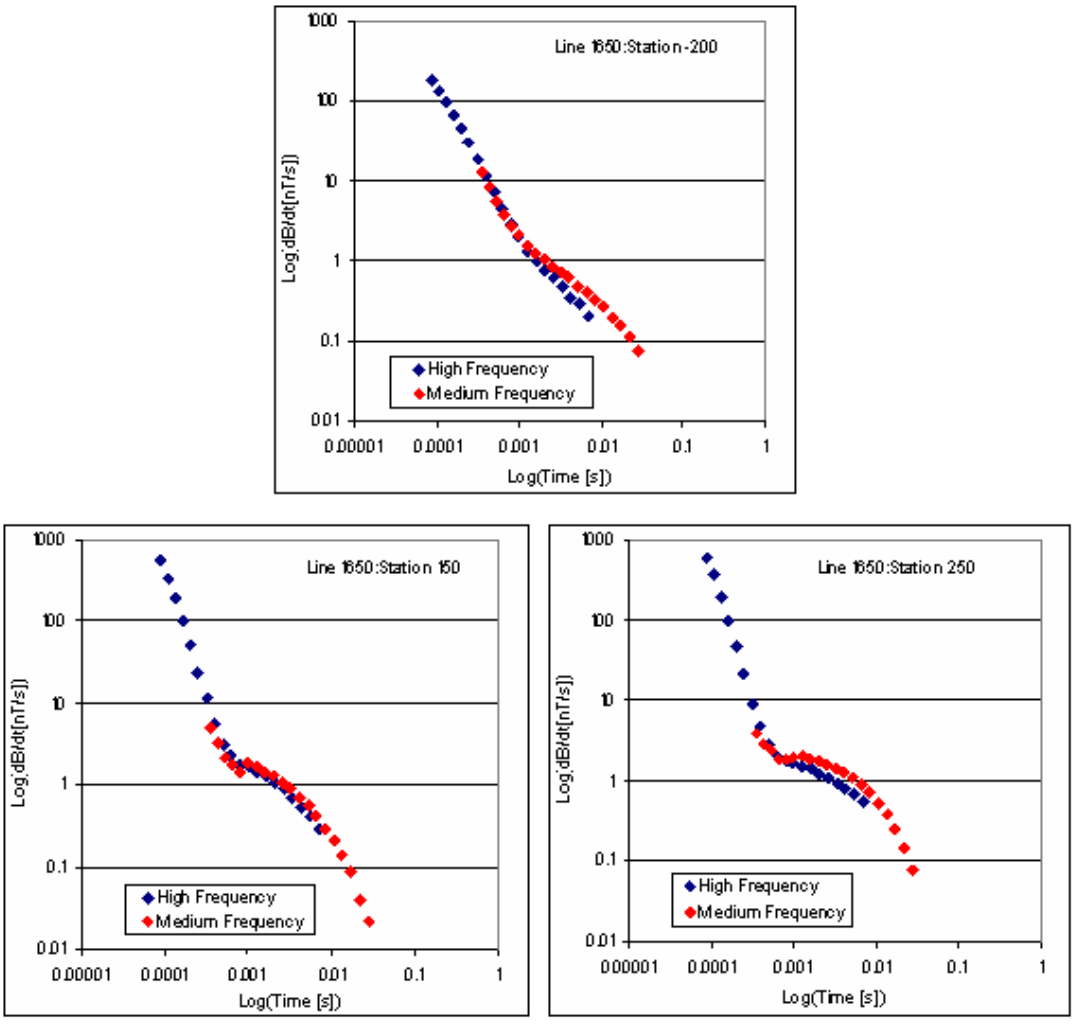

Figure 5-12: Line 1650; Stations -200, 150 and 250; medium and high frequency measured data.

5.2.5 Imaged conductivity sections

Figures 5-13 and 5-14 show screen dumps of a 3-D presentation of the complete data set as a series of imaged conductivity – depth sections plotted underneath the station positions which are draped over the DTM. The data set is attached in electronic format with Oasis Montaj Viewer where any combination of the sections can be displayed and viewed interactively in 3D. Also included is a colour contoured grid of the decay constant values determined as described in Chapter 4. Before contouring statistical inspection of the imaged conductivities still reveal a small number of erroneously high

values. A final filter is applied keeping only values between -5 and 5S/m to grid and contour. The contouring colour scheme is fixed for all sections and assigns dark blue to all negative values and a logarithmic scale from light blue (0S/m) to magenta (5S/m) for positive values. All negatives are grouped together as their presence can be used to help identify confined conductors and show instances where the assumptions of the S-layer differential transform were not completely satisfied, but there is little to be gained from the actual numerical value of these negative conductivities. It is therefore preferable to spread out the resolution of the colour contour scheme over the positive data range.

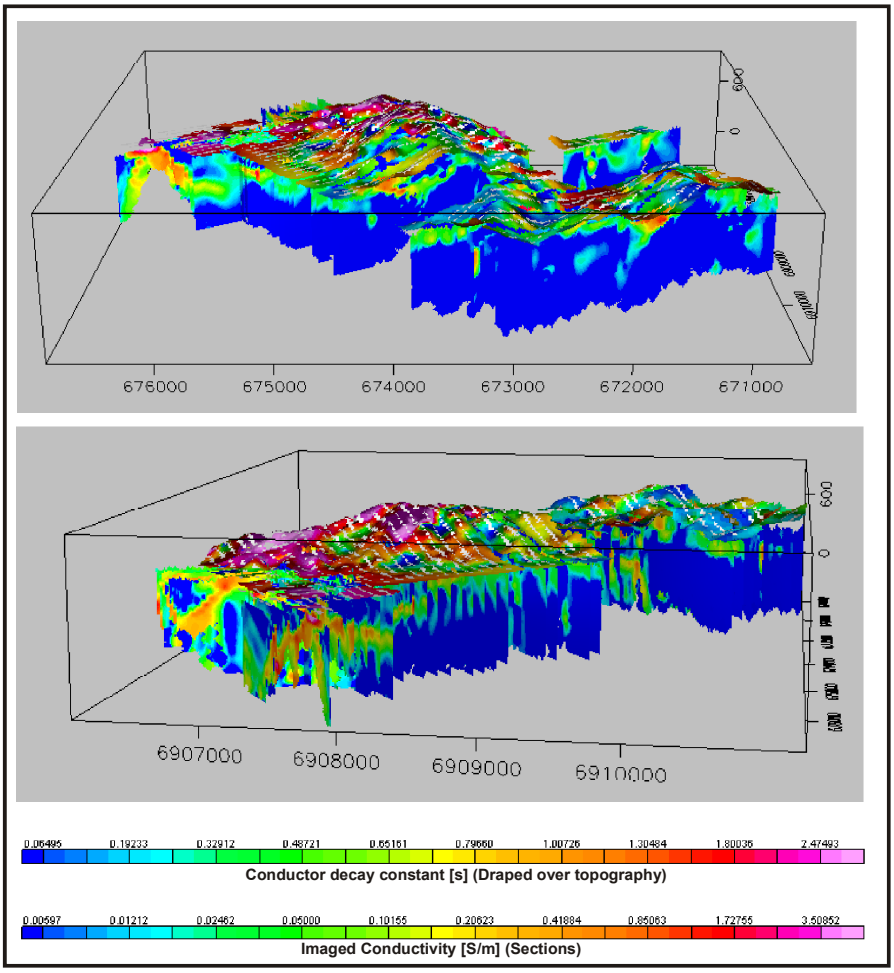

Figure 5-13: Contour map of conductor decay constants draped over topography and conductivity depth sections in 3D. Top viewpoint is from inclination 20˚, declination 180˚ and 5km distance. Bottom viewpoint is inclination 10˚, declination -100˚ and distance 5km. Axes are Northing, Easting and Elevation above sea level.

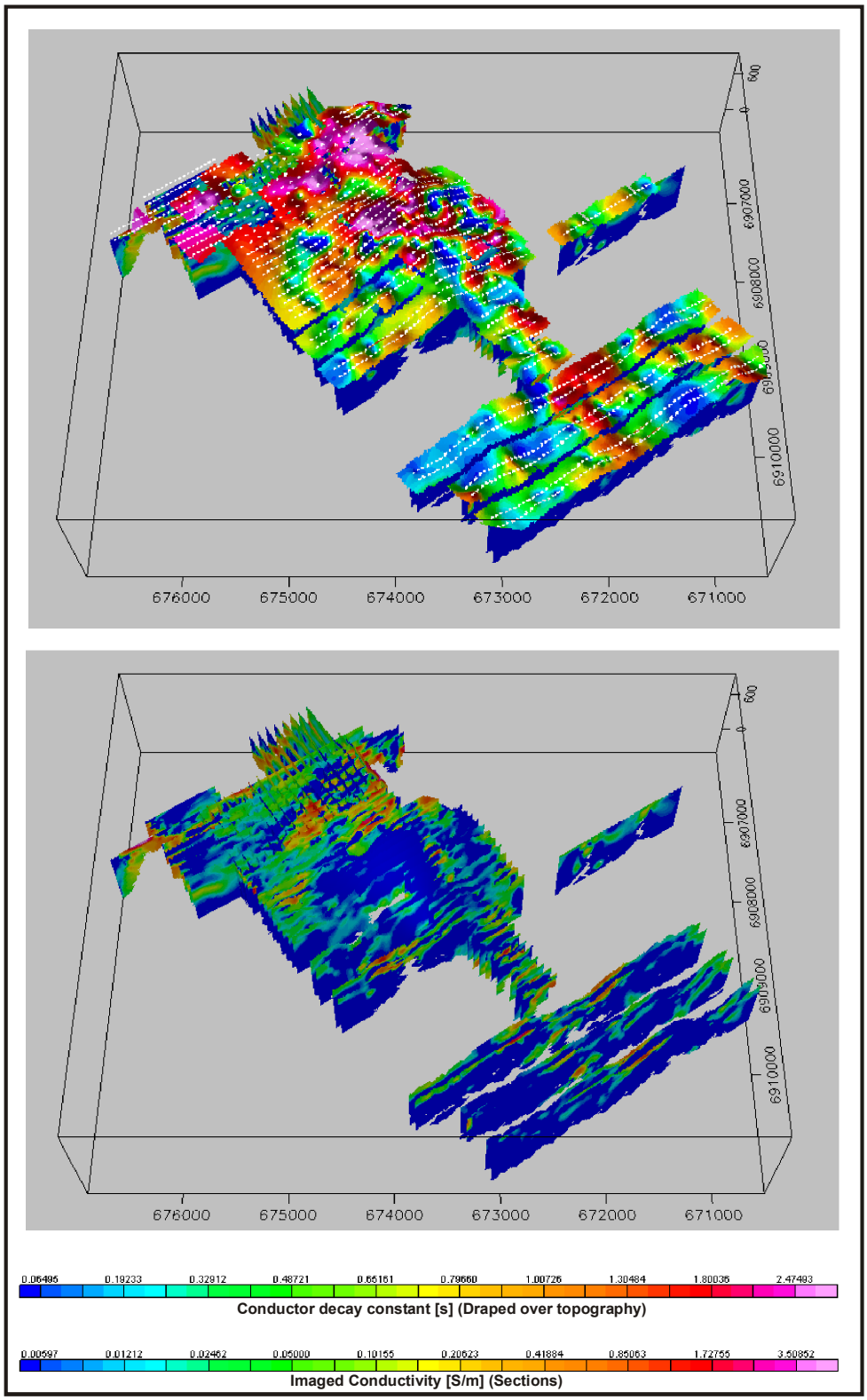

Figure 5-14: .3D view from inclination 60˚, declination 180˚ and 5km distance with and without contour map of conductor decay constants.

In the following section one area of interest will be isolated and compared with plate modelling results.

5.2.6 Comparison of automated conductor location with Maxwell plate model results

The results of the automated processing and conductor location of line 4050 are presented in Figure 5-15. At the very top, the profile data are shown for channels 1-10 and channels 11-20 respectively. On the late time profiles (channels 11-20) two prominent conductors are recognised, centred at stations -800m and 200m. These can also be identified on the conductivity depth section (second from top) as two near-surface conductors. However, there is a prominent conductor (station -300m) at depth that is not immediately evident on the profile plots. The conductor decay constants (third from the top) are displayed at scaled channels positions on the vertical axis and are not indicative of depths of conductors. All three conductors are mapped by the calculated decay constants with the deep conductor exhibiting the largest values. Decay constants of less than 0.5s are calculated on many stations, sometimes overlapping with half space decay behaviour and may be indicative of restraints in the automated algorithm that are chosen too loosely. Decay constants in this range can be ignored or filtered out. The bottom section indicates channels exhibiting power-law decay conforming to half space and S layer behaviour. These are found on stations where conductors are absent. An exception is stations -450m to -550m where half space behaviour is found on the first 5 channels and is replaced by the exponential decay in the later channels confirming the presence of a deep conductor. Figure 5-16 gives the same information for adjacent line 4150 and the close correlation between the sections for these two lines provides and indication of the stability that can be expected from the automated techniques. Figures 5-17 and 5-18 compares the conductivity depth sections with plate models that were produced with the Maxwell software package. The profiles at the top are channels 10-17 for the field and modelled data. The plate models have well-known inherent weaknesses in areas of complex geology but the correlation found with the conductivity depth sections confirms the conductor locations.

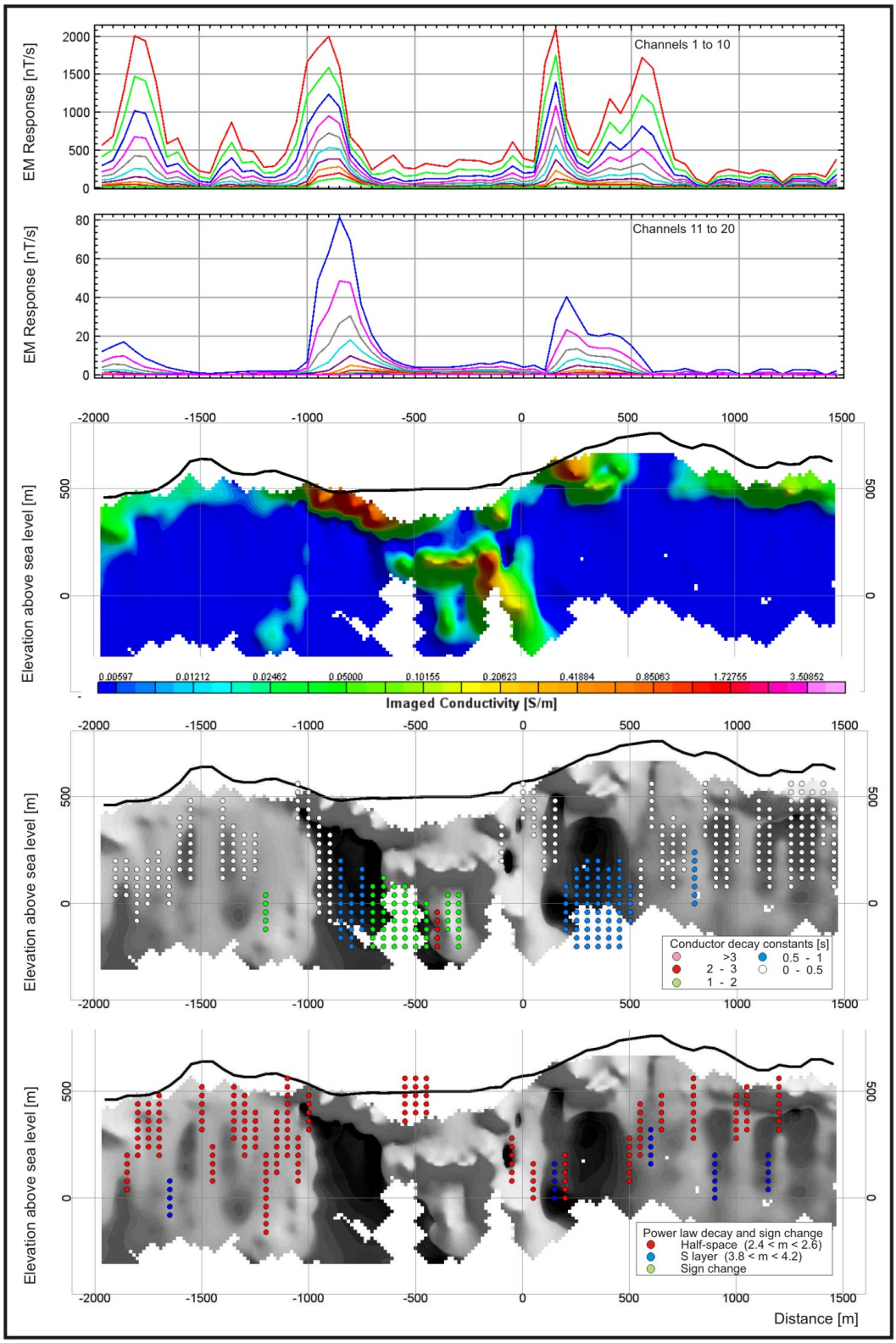

Figure 5-15: Line 4050. EM response profiles and sections from automated processing procedures.

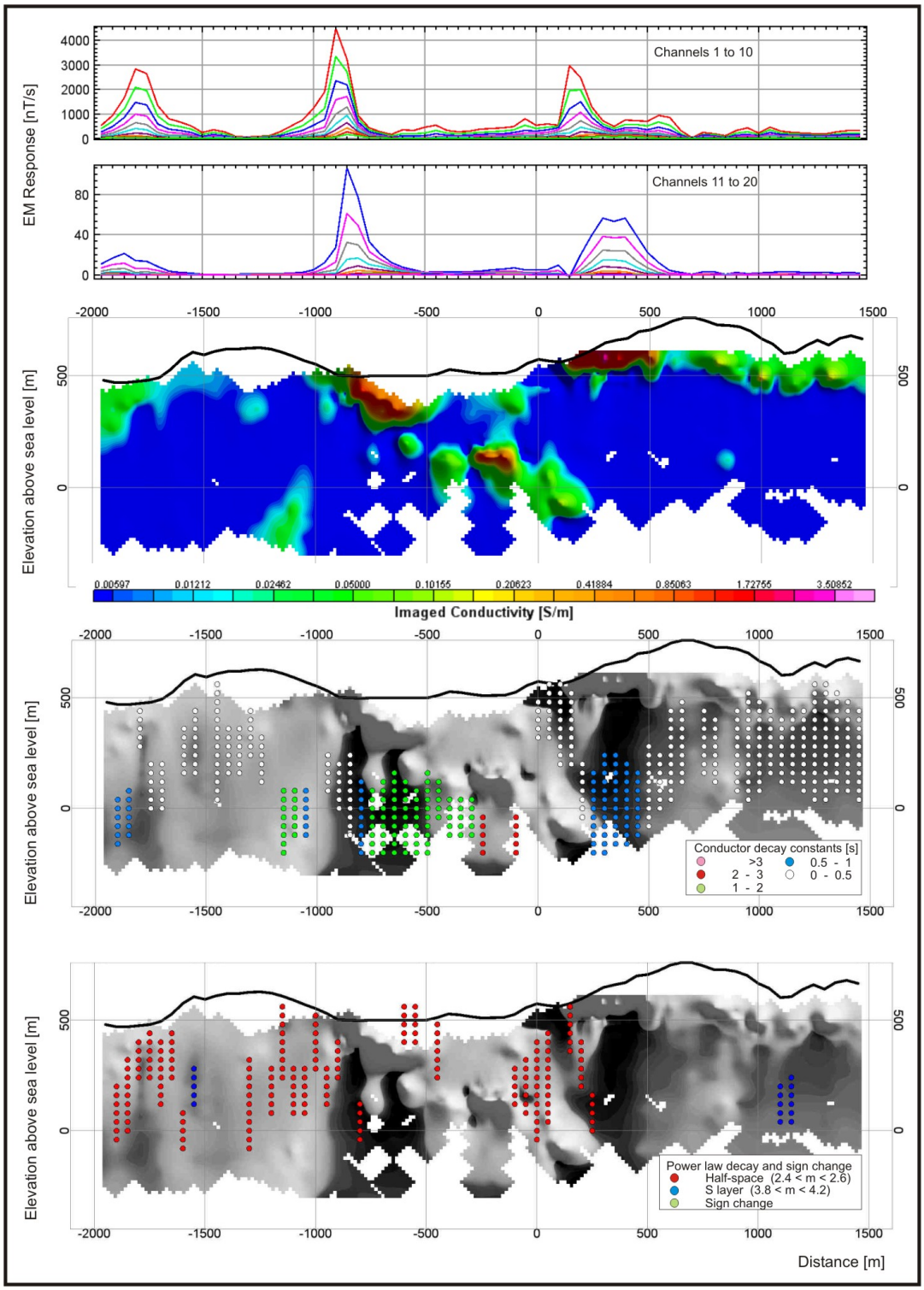

Figure 5-16: Line 4150. EM response profiles and sections from automated processing procedures.

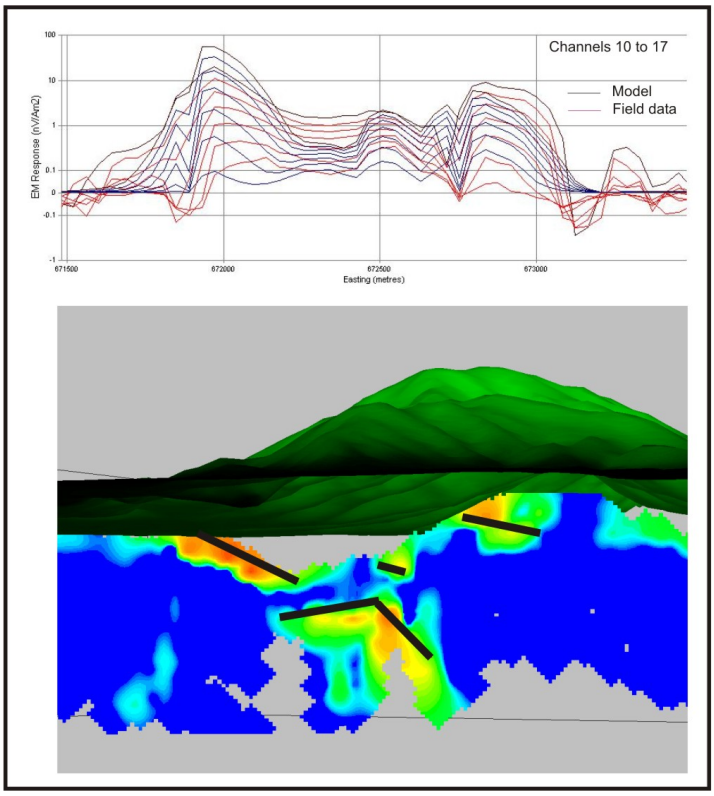

Figure 5-17: Line 4050. Comparison of Maxwell plate model and conductivity depth section.

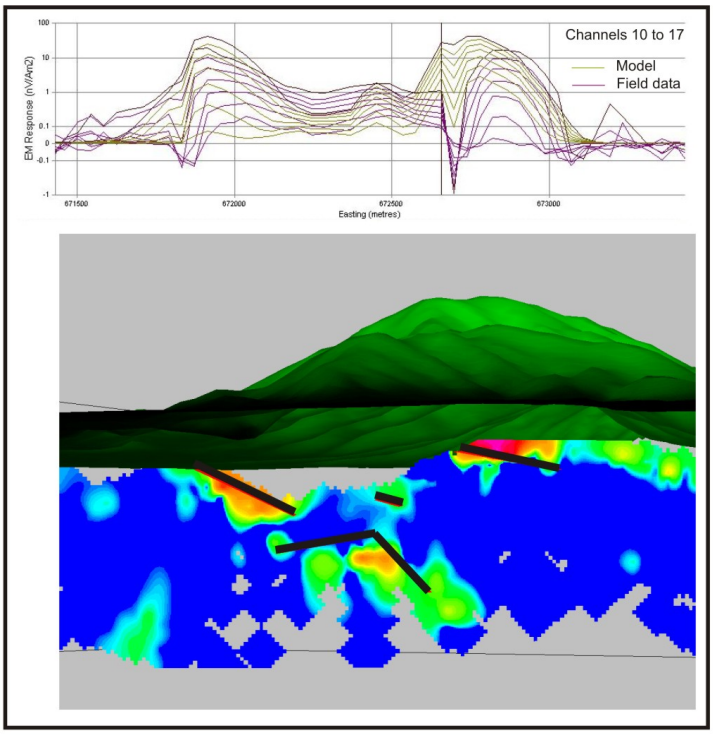

Figure 5-18: Line 4150. Comparison of Maxwell plate model and conductivity depth section.

5.3 Airborne survey

5.3.1 Data acquisition and system parameters

The airborne data were acquired with the VTEM system. The VTEM is a helicopter-borne TDEM system with central loop configuration developed by Geotech. One line is used to demonstrate the use of the S-layer transform. The data are presented here courtesy of BHP Billiton. Survey parameters are:

Transmitter Base Frequency Repetition Rate: 25

Transmitter Loop Diameter: 26m

Number of Turns: 4

Peak Current:: 170 A

Tx Dipole Moment: 361,000 NIA

Transmitter Wave Form: Trapezoid (with 40% duty cycle)

Receiver Loop Diameter: 1.1m

Rx Number of Turns: 60

Rx Time Gates: 27 ranging from 0.13ms to 8.9ms

Electromagnetic Receiver & serial number: Geotech VTEM 5

Electromagnetic Transmitter & serial number: Geotech VTEM 5

Length of cable for towed EM bird: 52

Height above ground for EM sensor: 80

The data is shown in Figure 5-19.

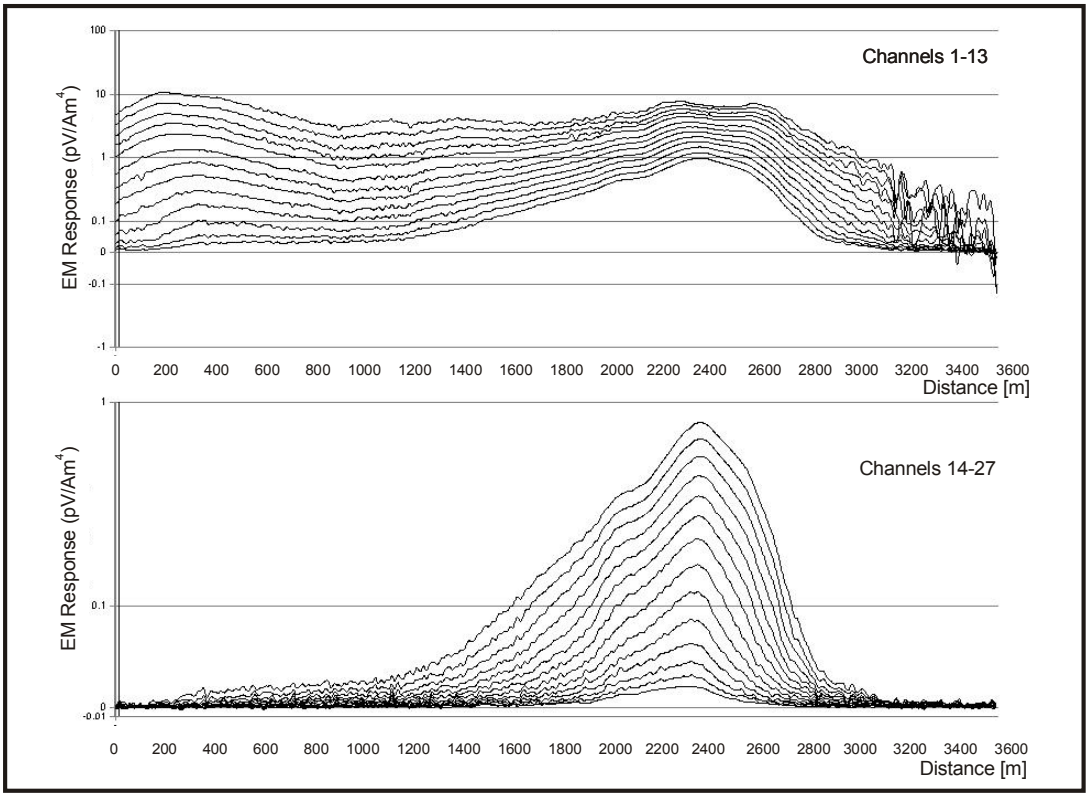

Figure 5-19: EM Response over conductor.

5.3.2 Automated processing

The conductivity depth section was calculated according to the same procedures set out in paragraph 5.2.3 and the conductor decay constants, half space decay behaviour and sign-changes determined as described in Chapter 4. The results are shown in Figures 5-20 to 5-23. The horizontal extent of the conductor is estimated to be from station 1700m to 2300m. The apparent extension of the conductor on either side can be explained in the same way as diffraction hyperbola phenomena on seismic sections. Stations not directly above the conductor will still measure its response, but data are plotted directly below the stations where it was measured, resulting in side "tails" on the conductivity depth sections. These effects are much more pronounced for dipping and vertical bodies. In this case it can be distinguished clearly based on the hyperbolic nature of the tail (station 2300m to 2800m), the corresponding drop in amplitude, and especially the "decrease of depth with increase of time" behaviour manifested as the white space

underneath the conductor where data not complying to the S-layer transform assumptions were filtered out (indicating high conductivity contrasts).

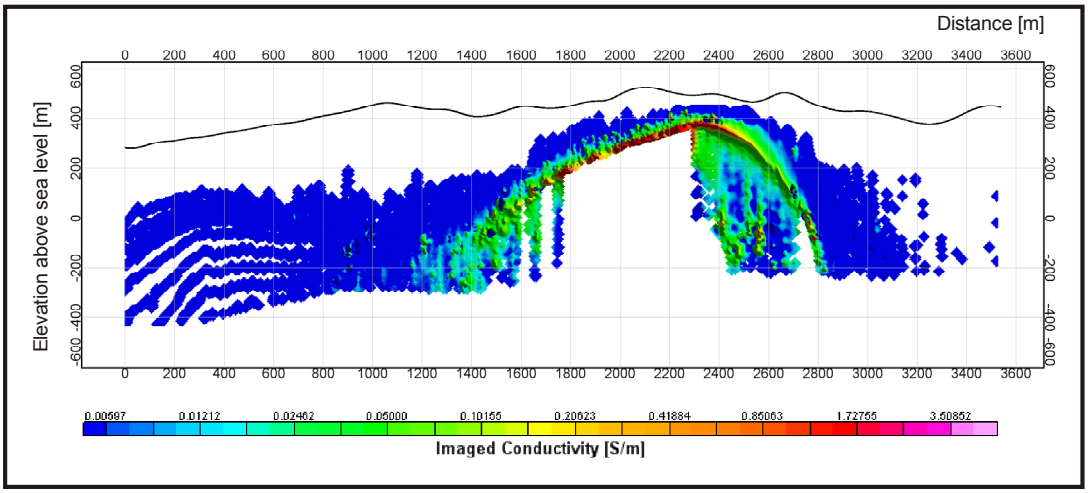

Figure 5-20: Conductivity depth section from S-layer transform, showing dipping conductor.

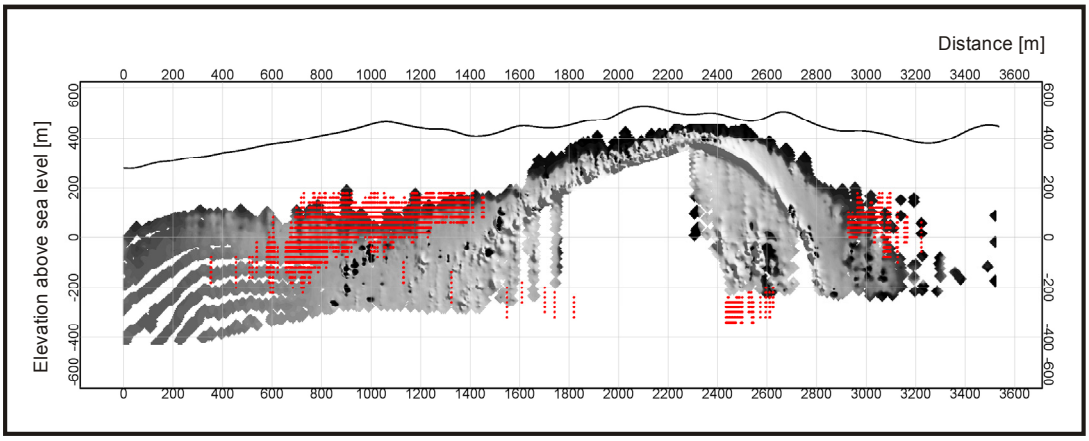

Figure 5-21: Conductivity depth section in greyscale with channels corresponding to half space power law decay indicated in red.

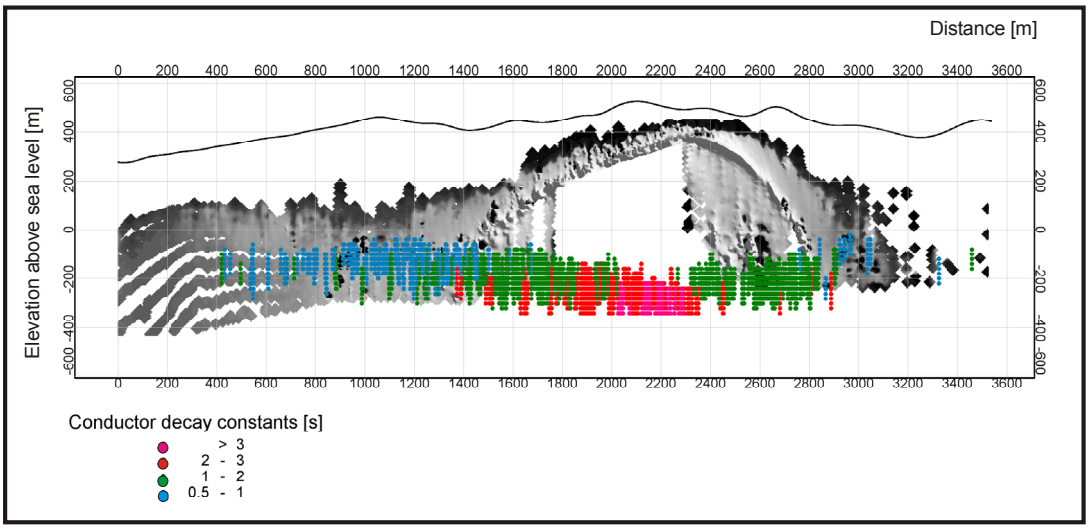

Figure 5-22: Conductivity depth section in greyscale with conductor decay constants plotted at scaled channel positions.

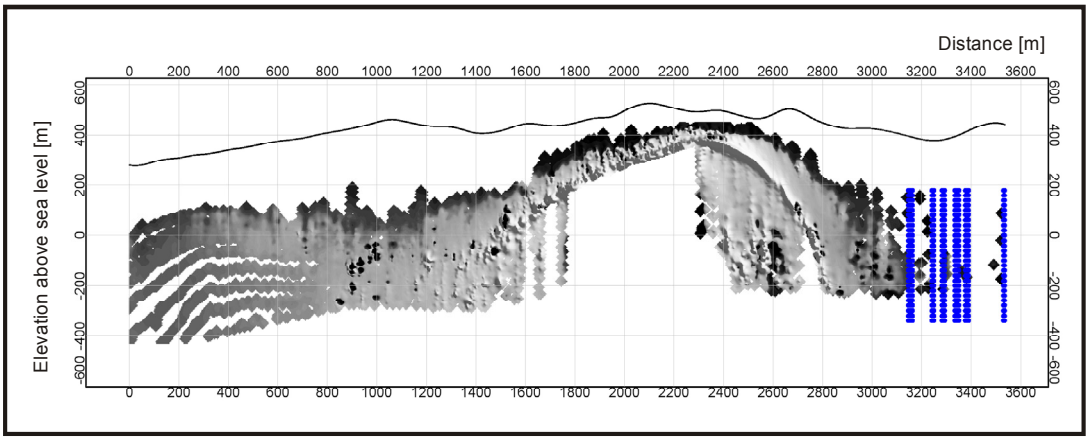

Figure 5-23: Conductivity depth section in greyscale with channels on stations showing sign changes indicated in blue.

The conductor decay constants plotted in Figure 5-22 also indicate maximum values on stations 1900m to 2400m, and if contoured the maximum of these values would correspond to the conductor location viewed in plan.

5.4 Conclusions and recommendations

The automated procedures outlined in chapter 4 can be implemented on both ground and airborne central loop configuration TDEM data. Filters to remove noise *as well as* clean data not conforming to the assumptions made in the S-layer differential transform can be applied efficiently in the time and spatial domains retaining the main advantage of the transform compared to inversion algorithms, namely speed. A combination of decay curve analysis and the S-layer differential transform allows sensitivity to both high conductivity contrast (well defined by exponential decay) and low contrast models (well defined by the S-layer transform). Care has to be taken when interpreting conductivity depth images, especially in the case of non-horizontal and especially near-vertical conductors as these will cause migration effects similar to that found in seismic sections. The procedures outlined in this work are considered to be completely automated since no starting model or information other than survey configuration and parameters are needed. Although the automated product is not considered to be a final interpretation it does provide very useful first phase identification of the subsurface conductivity.

Recommendations for further work are to:

- develop conductivity-depth section migration algorithms to correct for these effects
- test the effectiveness of the noise and SDTC filters on the more generalised inversion procedure described by Tartaras et. al. (2000)
- have borehole or other geological feedback in order to quantify the accuracy of the conductivity depth sections
- implement these, or similar algorithms, in TDEM instruments (such as a new generation metal detector) with the potential of real time imaging of data.